UNIVERSIDAD DE CONCEPCIÓN

Centro de Investigación en Ingeniería Matemática (CI^{2}MA)

Modelling the spatial-temporal evolution of the 2009 A/H1N1 influenza pandemic in Chile

Raimund Bürger, Gerardo Chowell,
Pep Mulet, Luis M. Villada

PREPRINT 2014-03

SERIE DE PRE-PUBLICACIONES

MODELLING THE SPATIAL-TEMPORAL EVOLUTION OF THE 2009 A/H1N1 INFLUENZA PANDEMIC IN CHILE

RAIMUND BÜRGER[A], GERARDO CHOWELL[B], PEP MULET[C], AND LUIS M. VILLADA[D]

Abstract. A spatial-temporal transmission model of 2009 A/H1N1 pandemic influenza across Chile, a country that spans a large latitudinal gradient, is developed to characterize the spatial variation in peak timing of the 2009 A/H1N1 influenza as a function of spatial connectivity assumptions across Chilean regions and the location of introduction of the virus into the country. The resulting model is a SEIR (susceptible-exposed-infected-removed) compartmental model with local diffusion and optional non-local terms to describe the migration of individuals of the S, E and R classes and the effect of a "hub region". This model is used along with epidemiological data to explore the spatial-temporal progression of pandemic influenza in Chile by assuming a range of transmission scenarios. Numerical results indicate that this relatively simple model is sufficient to characterize the south-north gradient observed during the 2009 influenza pandemic in Chile, and that the "hub region" corresponding to the capital region plays the critical role in keeping the population well mixed in a relatively short period of time.

1. Introduction

1.1. **Spatial-temporal variation of influenza.** Increasing our understanding of the spatial dissemination patterns of influenza is essential for public health surveillance and the implementation of reactive social distancing measures. Factors that have been associated with the spatial-temporal variation in seasonal influenza activity at the city or regional level include local environmental characteristics (e.g., temperature, specific humidity [1, 2] that enable local transmission, school cycles [3,4] whereby influenza transmission rates tend to decline during school breaks, as well as regional and global population mobility patterns [5–7]). For instance, a study based on 30 years of influenza-related mortality found a significant correlation between influenza activity across US states and the rates of movement of people to and from their workplaces (workflows) compared with geographical distance [5]. Another

Date: January 27, 2014.

Key words and phrases. SEIR model, influenza pandemic, spatial-temporal model, peak timing, transmission dynamics, hub region.

[a]CI^{2}MA and Departamento de Ingeniería Matemática, Facultad de Ciencias Físicas y Matemáticas, Universidad de Concepción, Casilla 160-C, Concepción, Chile. E-Mail: rburger@ing-mat.udec.cl.

[b]Mathematical and Computational Modeling Sciences Center, School of Human Evolution and Social Change, Arizona State University, Tempe, AZ 85287, USA, and Fogarty International Center National Institutes of Health, Bethesda, MD 20892, USA. E-Mail: gchowell@asu.edu.

[c]Departament de Matemàtica Aplicada, Universitat de València, Av. Dr. Moliner 50, E-46100 Burjassot, Spain. E-Mail: mulet@uv.es.

[d]CI^{2}MA and Departamento de Ingeniería Matemática, Facultad de Ciencias Físicas y Matemáticas, Universidad de Concepción, Casilla 160-C, Concepción, Chile. E-Mail: lmvillada@ing-mat.udec.cl.

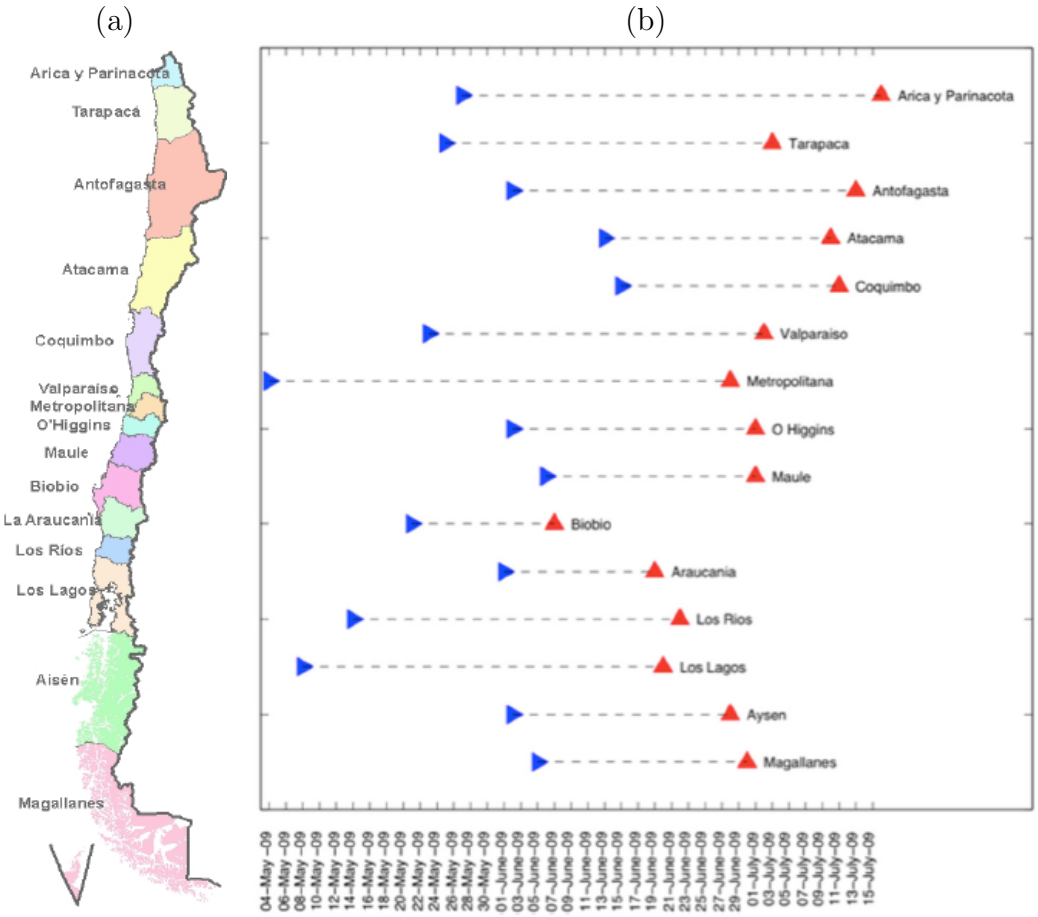

FIGURE 1. (a) Regions of Chile, (b) pandemic onset (denoted by symbol ▶) and pandemic peak (denoted by symbol ▲) timing across the 15 Chilean regions sorted from north (top) to south (bottom) Chile [14].

study using influenza hospitalization records among older adult populations across US states found a significant gradient in the peak timing of influenza at the state level whereby western states tended to peak earlier than northeastern states [8]. Similarly, another study based on weekly laboratory-confirmed influenza A from Canadian and US influenza surveillance systems showed a slight gradient in peak timing from the southwest regions in the US to northeast regions of Canada and the US. This study also found that regional influenza epidemics were more synchronized across the US (3–5 weeks) compared with Canada (5–13 weeks) [9].

1.2. **The 2009 A/H1N1 pandemic influenza in Chile.** In the context of the recent 2009 A/H1N1 influenza pandemic, population contact rates linked to school cycles or intervention strategies [10–12], demographic factors [13], local transmissibility [10, 11, 14], and global mobility patterns, which drives the timing of a virus's seeding across countries [15], have been associated with the complex spatial and temporal evolution of the 2009 A/H1N1 influenza

i	Name of Region i	Population	Area [km^2]	Length [km]
1	Arica y Parinacota	213816	16870	170
2	Tarapacá	300021	42220	265
3	Antofagasta	547463	126050	502
4	Atacama	292054	75200	399
5	Coquimbo	707654	40580	304
6	Vaparaíso	1734917	16400	113
7	Metropolitana	6685685	15400	105
8	O'Higgins	877784	16400	92
9	Maule	968336	30300	180
10	Biobío	1971998	37100	186
11	Araucanía	913065	31900	169
12	Los Ríos	364592	18500	131
13	Los Lagos	798141	48600	338
14	Aysén	99609	108500	602
15	Magallanes	159468	132300	644

TABLE 1. Official data for population and area for each region and approximate longitudinal length. Note that we number regions consecutively from north to south, and that these numbers do not correspond to the official Roman numerals assigned to the administrative regions of Chile.

pandemic. The 2009 A/H1N1 influenza pandemic spread as a single wave of transmission in Chile during the winter of 2009 soon after the first cases were confirmed in Mexico and California, USA [16]. The first two cases of novel 2009A/H1N1 influenza in Chile were confirmed in metropolitan Santiago on May 17, 2009 [16]. However, a retrospective study based on emergency room visit and laboratory viral surveillance conducted in southern city of Puerto Montt, capital of Los Lagos region, suggested that this city could have experienced a faster transmission rate and earlier pandemic onset by the end of April 2009 compared to the metropolitan area of Santiago [16]. Indeed, a recent study set in Chile showed that this country experienced a strong latitudinal gradient in pandemic peak timing in 2009, with southern regions experiencing earlier pandemic activity than northern regions [14], see Figure 1. Specifically, the southernmost regions (Biobío, Araucanía, Los Ríos, Los Lagos, Aysén, and Magallanes) peaked on average 16–39 days earlier relative to the northernmost region (Arica y Parinacota). This geographical variation in pandemic peak timing in Chile was found to be associated with differences in latitude and climatic conditions, with latitude, maximum temperature and specific humidity accounting for 69–80% of this variability in peak timing [14]. This south-north gradient in pandemic peak timing reported for Chile is consistent with a decreasing trend in transmissibility in the same direction, which was found to be statistically associated with maximum temperature and specific humidity. This is consistent with experimental studies suggesting that influenza transmission is more efficient under dry and cold conditions [2, 17–21].

1.3. **This contribution.** Here we develop a spatial-temporal transmission model of the 2009 A/H1N1 pandemic influenza across Chile, a country that spans a large latitudinal

gradient, to characterize the spatial variation in peak timing of influenza as a function of spatial connectivity assumptions across Chilean regions and the location of introduction of the virus into the country. We use epidemic modeling together with epidemiological data to explore the spatial-temporal progression of pandemic influenza in Chile by assuming a range of transmission scenarios to investigate the robustness of the south-north gradient observed during 2009 influenza pandemic in Chile.

The remainder of the paper is organized as follows. In Section 2, we describe the spatial-temporal SEIR (susceptible-exposed-infected-removed) model. In particular, in Section 2.1 we define its spatial version including local diffusion and, owing to the special geography of Chile, reduce the model to one space dimension. In Section 2.2 we perform a stability analysis for the case of constant diffusivity, starting from the well-known non-spatial version of the SEIR model which is given by a system of four coupled ordinary differential equations, with the result that whether the basic reproductive ratio R_0 is smaller or larger than one decides whether the disease-free state is locally asymptotically stable or unstable. Then, in Section 2.3 we define a generalization of the model to include a so-called "hub region", which is defined by a non-local convolution term. In Section 3 we outline the numerical scheme used for simulations. Then, in Section 4, we compare simulations obtained with the continuous model with diffusion and with/without migration via a hub region, which corresponds to the Chilean capital (metropolitan) region. We compute the number of infected individuals and estimate the "peak time", when the maximum concentration of infected is observed, in each region . These results are compared with the peak times observed in [14]. These results are discussed in Section 5.

2. Spatial-temporal SEIR model

Classical epidemiological models describe disease transmission on single populations of individuals by aggregating all of the members into one of four different classes. However, these single population models rely on the strong assumption that the entire population is mixing homogeneously and they offer no information about the spread of the disease across regions, which is reasonable in small areas but does not well reflect reality across large geographic regions.

2.1. **Spatial domain and governing equations.**

We consider one country identified by a bi-dimensional domain $\Omega \subset \mathbb{R}^2$, where $\boldsymbol{x} = (x, y)$ and x and y are latitudinal and longitudinal coordinates, respectively, measured in kilometers. We assume that Ω is simply connected and has a continuous, piecewise smooth boundary $\partial\Omega$ with a normal $\boldsymbol{n} = \boldsymbol{n}(\boldsymbol{x})$.

We consider the classical epidemical SEIR model proposed by Kermack and McKendrick [22] with standard incidence [23] (see also [24–29]). This model keeps track of four classes of individuals at time t and the location $\boldsymbol{x} \in \Omega$, the density of susceptibles $S(\boldsymbol{x}, t)$, the density of exposed $E(\boldsymbol{x}, t)$ in which individuals are in the latent period, the density of infectives $I(\boldsymbol{x}, t)$ in which individuals are infectious and the density of recovered $R(\boldsymbol{x}, t)$ that keeps track of individuals removed from the infected compartment. We start from the following assumptions.

(1) The population is constant (without births or deaths, and the disease is assumed non-letal), i.e.

$$\int_\Omega N(\boldsymbol{x},t)\,\mathrm{d}\boldsymbol{x} = N_0 \quad \text{for all } t \geq 0,$$

where the population density is $N = S + E + I + R$.

(2) The transmission is described by local standard incidence. Thus, for each $\boldsymbol{x} \in \Omega$, once an infected individual is introduced into the susceptible area and contacts a sufficient number of susceptibles at time t, the fraction of new infected individuals per unit time is $\beta(\boldsymbol{x})S(\boldsymbol{x},t)/N(\boldsymbol{x},t)$, where $\beta(\boldsymbol{x})$ is the local transmission coefficient. The number of new infected individuals per unit time resulting in each point $\boldsymbol{x} \in \Omega$ at time t is $\beta(\boldsymbol{x})S(\boldsymbol{x},t)I(\boldsymbol{x},t)/N(\boldsymbol{x},t)$.

(3) The number of individuals recovered from the infected class per unit time at $\boldsymbol{x} \in \Omega$ and at time t is $\gamma I(\boldsymbol{x},t)$, where γ is the rate constant for recovery, corresponding to a mean infectious period of $1/\gamma$.

(4) Individuals of each class disperse by means of Fickian diffusion throughout Ω. Precisely, and let $-d_P(\boldsymbol{x})\nabla P$ be the population flux, where $d_P(\boldsymbol{x}) \geq 0$ is the space-dependent diffusion coefficient for $P \in \{S, E, R\}$. Thus, individuals are assumed to move an in undirected manner across the entire region and to contact only those individuals in their immediate area. Infected individuals are not allowed to move.

(5) At any time the population in Ω is isolated.

Based on these assumptions, we obtain the following model:

$$\begin{aligned}
\frac{\partial S}{\partial t} &= -\beta(\boldsymbol{x})\frac{SI}{N} + \nabla\cdot\big(d_S(\boldsymbol{x})\nabla S\big),\\
\frac{\partial E}{\partial t} &= \beta(\boldsymbol{x})\frac{SI}{N} - \kappa E + \nabla\cdot\big(d_E(\boldsymbol{x})\nabla E\big),\\
\frac{\partial I}{\partial t} &= \kappa E - \gamma I,\\
\frac{\partial R}{\partial t} &= \gamma I + \nabla\cdot\big(d_R(\boldsymbol{x})\nabla R\big).
\end{aligned} \tag{2.1}$$

A sufficient condition for an isolated population is a zero-flux boundary condition for $P \in \{S, E, I, R\}$, which leads to the homogeneous Neumann boundary conditions

$$\frac{\partial S}{\partial \boldsymbol{n}}(\boldsymbol{x},t) = \frac{\partial E}{\partial \boldsymbol{n}}(\boldsymbol{x},t) = \frac{\partial R}{\partial \boldsymbol{n}}(\boldsymbol{x},t) = 0 \quad \text{for } \boldsymbol{x} \in \partial\Omega \text{ and } t > 0,$$

where $\boldsymbol{n}$ denotes the unit exterior normal vector to the boundary $\partial\Omega$ of Ω at position $\boldsymbol{x}$ and, as usual, $\partial S/\partial \boldsymbol{n} = \nabla S \cdot \boldsymbol{n}$, etc. Thus, the total number of individuals at time t,

$$N_{\mathrm{tot}}(t) := \int_\Omega N(\boldsymbol{x},t)\,\mathrm{d}\boldsymbol{x},$$

is actually constant, i.e., $N_{\mathrm{tot}}(t) = N_{\mathrm{tot}}(t_0) = N_0$, since

$$\frac{\mathrm{d}}{\mathrm{d}t}N_{\mathrm{tot}}(t) = \int_\Omega \left(\sum_{P\in\{S,E,I,R\}} \frac{\partial}{\partial t}P(\boldsymbol{x},t)\right)\mathrm{d}\boldsymbol{x} = \int_\Omega \left(\sum_{P\in\{S,I,R\}} \nabla\cdot\big(d_P(\boldsymbol{x})\nabla P\big)\right)\mathrm{d}\boldsymbol{x} = 0.$$

For the particular geographic reality of countries that mainly extend in the direction of only one of the coordinate axes (an assumption obviously motivated by the geography of Chile, but which may include a few other places as well), a significant model reduction but with an acceptable loss of realism can be achieved if we reduce the model (2.1) to one space dimension. Thus, we obtain the following system:

$$\begin{aligned}
\frac{\partial S}{\partial t} &= -\beta(x)\frac{S(x,t)I(x,t)}{N(x,t)} + \frac{\partial}{\partial x}\left(d_S(x)\frac{\partial S}{\partial x}(x,t)\right),\\
\frac{\partial E}{\partial t} &= \beta(x)\frac{S(x,t)I(x,t)}{N(x,t)} - \kappa E(x,t) + \frac{\partial}{\partial x}\left(d_E(x)\frac{\partial E}{\partial x}(x,t)\right),\\
\frac{\partial I}{\partial t} &= \kappa E(x,t) - \gamma I(x,t),\\
\frac{\partial R}{\partial t} &= \gamma I(x,t) + \frac{\partial}{\partial x}\left(d_R(x)\frac{\partial R}{\partial x}(x,t)\right),
\end{aligned} \tag{2.2}$$

which is supplemented by initial conditions.

2.2. **Stability analysis.** To discuss the stability properties of (2.1), let us briefly recall well-known results for the standard (non-spatial) SEIR model, which is recovered by setting $d_P \equiv 0$, $P \in \{S, E, R\}$, in (2.1). We select the version of the model defined at position x (as by the choice of $\beta(x)$), and consider for a moment x as a parameter, i.e. we study the ODE model

$$\begin{aligned}
\frac{\mathrm{d}S(t;x)}{\mathrm{d}t} &= -\beta(x)\frac{S(t;x)I(t;x)}{N(t;x)},\\
\frac{\mathrm{d}E(t;x)}{\mathrm{d}t} &= \beta(x)\frac{S(t;x)I(t;x)}{N(t;x)} - \kappa E(t;x),\\
\frac{\mathrm{d}I(t;x)}{\mathrm{d}t} &= \kappa E(t;x) - \gamma I(t;x),\\
\frac{\mathrm{d}R(t;x)}{\mathrm{d}t} &= \gamma I(t;x).
\end{aligned} \tag{2.3}$$

For the model (2.3) we define the *basic reproductive ratio* associated with position x by

$$R_0(x) := \beta(x)/\gamma.$$

If $R_0(x) > 1$ for $\boldsymbol{x} \in \Omega$, then the disease-free steady state at position x is unstable so that an epidemic may potentially occur. If that happens then $I(t;\boldsymbol{x})$ first increases to a maximum attained when $S(t;\boldsymbol{x}) = \gamma N(t;\boldsymbol{x})/\beta(\boldsymbol{x})$, and then decreases to zero. On the other hand, if $R_0(\boldsymbol{x}) < 1$ for $\boldsymbol{x} \in \Omega$, then the disease-free steady state at x is stable so that the disease dies out, i.e., $I(t,\boldsymbol{x})$ decreases to zero at $x \in \Omega$.

We now perform a linearized stability analysis for the one-dimensional system (2.2) with $d_P(x) := d$ for $\in \{S, E, R\}$ and $\beta(x) = \beta$. With this goal, we rewrite (2.2) in the form

$$\boldsymbol{u}_t = \boldsymbol{g}(\boldsymbol{u}) + d\boldsymbol{D}\boldsymbol{u}, \tag{2.4}$$

where $\boldsymbol{u} = (S, E, I, R)^{\mathrm{T}}$, $\boldsymbol{g}(\boldsymbol{u})$ corresponds to the reactive term in the SEIR model, and

$$\boldsymbol{D} = \operatorname{diag}\left(\frac{\partial^2}{\partial x^2}, \frac{\partial^2}{\partial x^2}, 0, \frac{\partial^2}{\partial x^2}\right). \tag{2.5}$$

The linearized equation for a small perturbation $\boldsymbol{v}$ about an equilibrium point $\boldsymbol{u}^{(0)}$ of the dynamical system $\boldsymbol{u}' = \boldsymbol{g}(\boldsymbol{u})$ is obtained by substituting $\boldsymbol{u} = \boldsymbol{u}^{(0)} + \boldsymbol{v}$ into (2.4) and neglecting second order terms in $\boldsymbol{v}$. This yields the following linearized version of (2.4):

$$\boldsymbol{v}_t = \boldsymbol{g}'(\boldsymbol{u}^{(0)})\boldsymbol{v} + d\boldsymbol{D}\boldsymbol{v}. \tag{2.6}$$

We consider $\boldsymbol{u}^{(0)} = (s_0, 0, 0, 0)^{\mathrm{T}}$ with $s_0 > 0$.

We now seek solutions of (2.6) of the form $\boldsymbol{v}(x,t) = \boldsymbol{z}(t;\xi)\exp(\mathrm{i}\xi x)$ for a fixed frequency ξ. The vector function $\boldsymbol{z}$ satisfies the system of ordinary differential equations

$$\boldsymbol{z}' = \boldsymbol{M}\big(\boldsymbol{u}^{(0)};\xi\big)\boldsymbol{z},$$

where we define the matrix

$$\boldsymbol{M}\big(\boldsymbol{u}^{(0)};\xi\big) := \boldsymbol{g}'\left(\boldsymbol{u}^{(0)}\right) - \xi^2 d\boldsymbol{I}_*,$$

where $\boldsymbol{I}_* = \operatorname{diag}(1,1,0,1)$ and

$$\boldsymbol{g}'\big(\boldsymbol{u}^{(0)}\big) = \begin{bmatrix} 0 & 0 & -\beta & 0 \\ 0 & -\kappa & \beta & 0 \\ 0 & \kappa & -\gamma & 0 \\ 0 & 0 & \gamma & 0 \end{bmatrix}.$$

The linearized asymptotical stability of $\boldsymbol{u}^{(0)}$ is equivalent to $\lim_{t\to\infty}\boldsymbol{z}(t,\xi) = 0$ for all ξ, and this is equivalent to $\operatorname{Re}\lambda < 0$ for any eigenvalue λ of $\boldsymbol{M}(\boldsymbol{u}^{(0)};\xi)$ and any $\xi \in \mathbb{R}$. The eigenvalues of $\boldsymbol{M}(\boldsymbol{u}^{(0)};\xi)$ are $\lambda_{1,2} = -\xi^2 d$ and

$$\lambda_{3,4} = \frac{1}{2}\big(-(\gamma+\kappa+d\xi^2) \pm \sqrt{(\gamma+\kappa+d\xi^2)^2 - 4(\kappa(\gamma-\beta)+\gamma d\xi^2)}\big),$$

so that $\operatorname{Re}\lambda_{3,4} < 0$ if and only if $\kappa(\gamma-\beta)+\gamma d\xi^2 > 0$. Therefore we have proved the following lemma.

Lemma 1. *The equilibrium point $\boldsymbol{u}^{(0)}$ is locally asymptotically stable for the model (2.2) if $R_0 = \beta/\gamma < 1$ and unstable if $R_0 > 1$.*

2.3. **Continuous model with a hub region.** For certain subpopulation $u \in \{S, E, R\}$, a constant non-local migration can be represented by the following equation:

$$\begin{aligned} \frac{\partial u}{\partial t} &= g(\boldsymbol{u}) + \frac{\partial}{\partial x}\left(d(x)\frac{\partial u}{\partial x}\right) \\ &\quad + \int_0^L K(z,x)u(z,t)\,\mathrm{d}z - \int_0^L K(x,z)u(x,t)\,\mathrm{d}z, \quad x \in [0,L], \quad t > 0, \end{aligned} \tag{2.7}$$

where $[x_a, x_b]$ is certain *hub region* and

$$K(x,y) = \begin{cases} \nu \text{ if } x \in [x_a,x_b] \text{ or } y \in [x_a,x_b], \\ 0 \text{ otherwise,} \end{cases}$$

is the function that indicates the rate of individuals at x that move to y. The first integral in (2.7) corresponds to migration from the hub region to a point x at rate ν, while the second integral corresponds to migration of population from x to the hub region at rate ν. Observe that

$$\int_0^L \left(\int_0^L K(z,x)u(z,t)\,\mathrm{d}z - \int_0^L K(x,z)u(x,t)\,\mathrm{d}z \right) \mathrm{d}x = 0, \quad u \in \{S,E,I,R\},$$

therefore the total population remains constant.

3. Numerical scheme

We consider the domain $[0,L]$ of length $L = 4200$, which is approximately the length of continental Chile in kilometers. For grid points $x_j := (j - \frac{1}{2})\Delta x$ for $j = 1,\ldots,M$, where $\Delta x := L/M$, and $t_n := n\Delta t$ for $n \in \mathbb{N}_0$, we calculate approximate values $u_j^n \approx u(x_j,t_n)$ for $u \in \{S,E,I,R\}$. We denote $\boldsymbol{u}_j^n = (S_j^n, E_j^n, I_j^n, R_j^n)^{\mathrm{T}}$ and $\boldsymbol{u}^n = (\boldsymbol{u}_1^n,\ldots,\boldsymbol{u}_M^n)^{\mathrm{T}}$.

The continuous model (2.2), supplied with suitable initial conditions, is solved numerically by an explicit-implicit Euler method, for which the reaction is discretized explicitly, while an implicit discretization is used for the diffusive part in the continuous model. (This method is the simplest variant of the so-called IMEX schemes for convection-diffusion problems, see [30].) The resulting scheme is

$$\boldsymbol{u}^{n+1} = \boldsymbol{u}^n + \Delta t\big(\boldsymbol{G}(\boldsymbol{u}^n,\boldsymbol{x}) + d\boldsymbol{D}_{\Delta x}\boldsymbol{u}^{n+1}\big), \quad n = 0,1,\ldots,$$

where $\boldsymbol{G}(\boldsymbol{u}^n,\boldsymbol{x})$ is a vector of $4M$ components given by

$$\boldsymbol{G}(\boldsymbol{u}^n,\boldsymbol{x}) = \begin{pmatrix} \boldsymbol{g}(\boldsymbol{u}_1^n, x_1) \\ \boldsymbol{g}(\boldsymbol{u}_2^n, x_2) \\ \vdots \\ \boldsymbol{g}(\boldsymbol{u}_M^n, x_M) \end{pmatrix},$$

where

$$\boldsymbol{g}\big((S,E,I,R)^{\mathrm{T}},x\big) = \begin{pmatrix} -\beta(x)SI/N \\ \beta(x)SI/N - \kappa E \\ \kappa E - \gamma I \\ \gamma I \end{pmatrix}, \quad N = S+E+I+R,$$

and $\boldsymbol{D}_{\Delta x}$ is the $(4M)\times(4M)$ matrix that discretizes (2.5):

$$\boldsymbol{D}_{\Delta x} = L_{\Delta x} \otimes \boldsymbol{I}_*, \quad \boldsymbol{I}_* = \mathrm{diag}(1,1,0,1),$$

where $L_{\Delta x}$ denotes the usual discretization of the 1D Laplacian with Neumann boundary conditions on an M-grid over the spatial domain $[0,L]$ with cell size $\Delta x = L/M$.

The model with non-local migration (2.7) is discretized in a similar way. In this case the non-local migration term is treated explicitly:

$$\boldsymbol{u}^{n+1} = \boldsymbol{u}^n + \Delta t\big(\boldsymbol{G}(\boldsymbol{u}^n,\boldsymbol{x}) + d\boldsymbol{D}_{\Delta x}\boldsymbol{u}^{n+1} + \boldsymbol{H}_{\mathrm{hub}}(\boldsymbol{u}^n)\big), \quad n = 0,1,\ldots,$$

where $\boldsymbol{H}_{\text{hub}}(\boldsymbol{u}^n)$ is a vector of $4M$ components that approximates the integral terms in (2.7) by the midpoint rule:

$$\boldsymbol{H}_{\text{hub}}(\boldsymbol{u}^n) = \begin{pmatrix} (\boldsymbol{H}_{\text{hub}}(\boldsymbol{u}^n))_1 \\ (\boldsymbol{H}_{\text{hub}}(\boldsymbol{u}^n))_2 \\ \vdots \\ (\boldsymbol{H}_{\text{hub}}(\boldsymbol{u}^n))_M \end{pmatrix},$$

where

$$(\boldsymbol{H}_{\text{hub}}(\boldsymbol{u}^n))_i = \Delta x \left(\sum_{j=1}^{M} K(x_j, x_i)\boldsymbol{u}_j^n - \sum_{j=1}^{M} K(x_i, x_j)\boldsymbol{u}_i^n \right).$$

In the simulations we use $M = 1000$ and $\Delta t = 0.1\,\text{d}$, since we have checked that more resolution does not significantly change the simulation.

4. Numerical simulations

4.1. **Epidemiological and population data.** We relied on a large individual-level dataset comprising all hospitalizations for severe acute respiratory infection (hereafter referred to as SARI) reported by all public and private hospitals to the Chilean Ministry of Health during 01-May to 31-December 2009 to characterize peak timing across Chilean regions.

A total of 1809 SARI hospitalizations (29.4%) were laboratory confirmed with A/H1N1 pandemic influenza. We obtained regional estimates of population size for 2009 from the Instituto Nacional de Estadísticas [31].

We consider the initial population according to official data to December 2011 (see [14]) and assume a constant distribution of population along its geographical localization for each region based on official data that are tabulated in Table 1.

4.2. **Initial values and constants.** It is difficult to determine suitable values for $E(x, 0)$ and $I(x, 0)$ that would allow us to obtain similar results as those reported in [14]. We therefore tested four different initial conditions corresponding to different scenarios. "Scenario i" corresponds to one infected individual uniformly distributed along region i and zero infected individuals in all other regions. The number of individuals of class $P \in \{S, E, I, R\}$ in region $i \in \{1, \ldots, 15\}$ at time t is computed as

$$P_i(t) = \int_{l_i} P(x, t)\,\text{d}x,$$

where l_i is the latitude interval corresponding to region i. The number of individuals newly infected in the time interval $[t-1, t]$ (t measured in days) in region i is calculated as

$$I_i^{\text{new}}(t) = \int_{t-1}^{t} \kappa E_i(\tau)\,\text{d}\tau.$$

The constants are chosen as $1/\kappa = 2\,\text{d}$ and $1/\gamma = 4\,\text{d}$, $\kappa = 0.5\,\text{d}^{-1}$ and $\gamma = 0.25\,\text{d}^{-1}$. Moreover we choose $d = 10\,\text{km}^2/\text{d}$ and $\nu = 10^{-5}\,\text{d}^{-1}$.

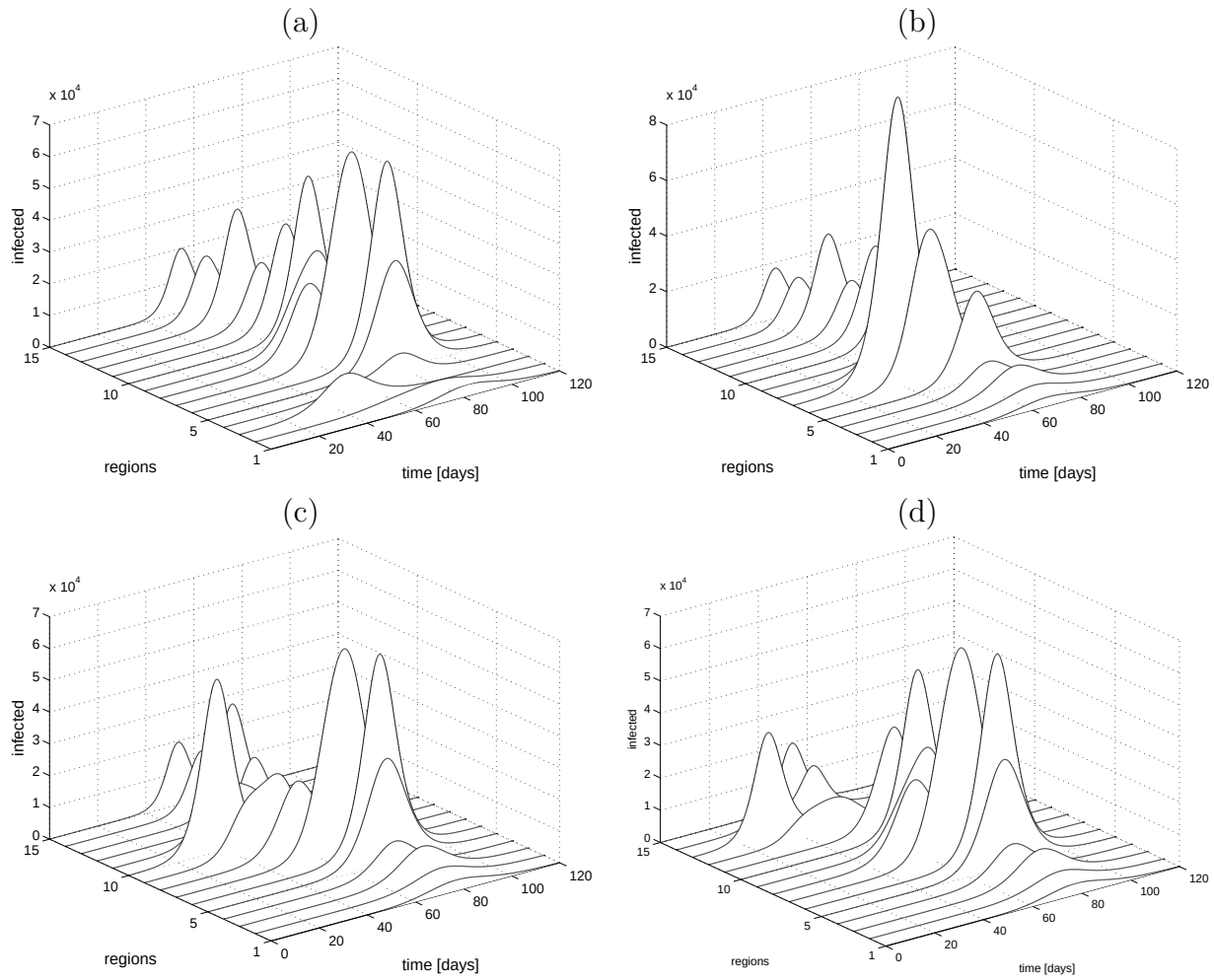

FIGURE 2. Simulation of disease spread for four different initial scenarios with $d(x) = 10$, $\nu = 1 \times 10^{-5}$ and $R_0(x) > 1$: (a) Scenario 3, (b) Scenario 7, (c) Scenario 10, (d) Scenario 13.

4.3. **Case $R_0(x) > 1$ for $x \in [0, L]$.** In this case the local transmission coefficient $\beta(x)$ is set such that $R_0(x) = \beta(x)/\gamma$ satisfies $R_0(0) = 1.2$ (northernmost region) and increases linearly as a function of space until $R_0(L) = 1.6$ (southernmost region) i.e.

$$\beta(x) = \frac{x}{10L} + 0.3, \quad 0 \leq x \leq L.$$

According to Lemma 1 in Section 2.2 any point in the domain is a endemic point.

In Figures 2 and 3 the disease spread for different initial scenarios is shown. In Figure 4 the peak times of simulations for different scenarios are shown and compared with the peak timing reported in [14]. Scenarios 10 and 13 give a good fit to the experimental data, thus pointing that the epidemic might have started in southern Chile. Since the local reproductive number increases from southern to northern regions in our model, the attack rates shown in Figure 3 also increase in the same direction as R_0.

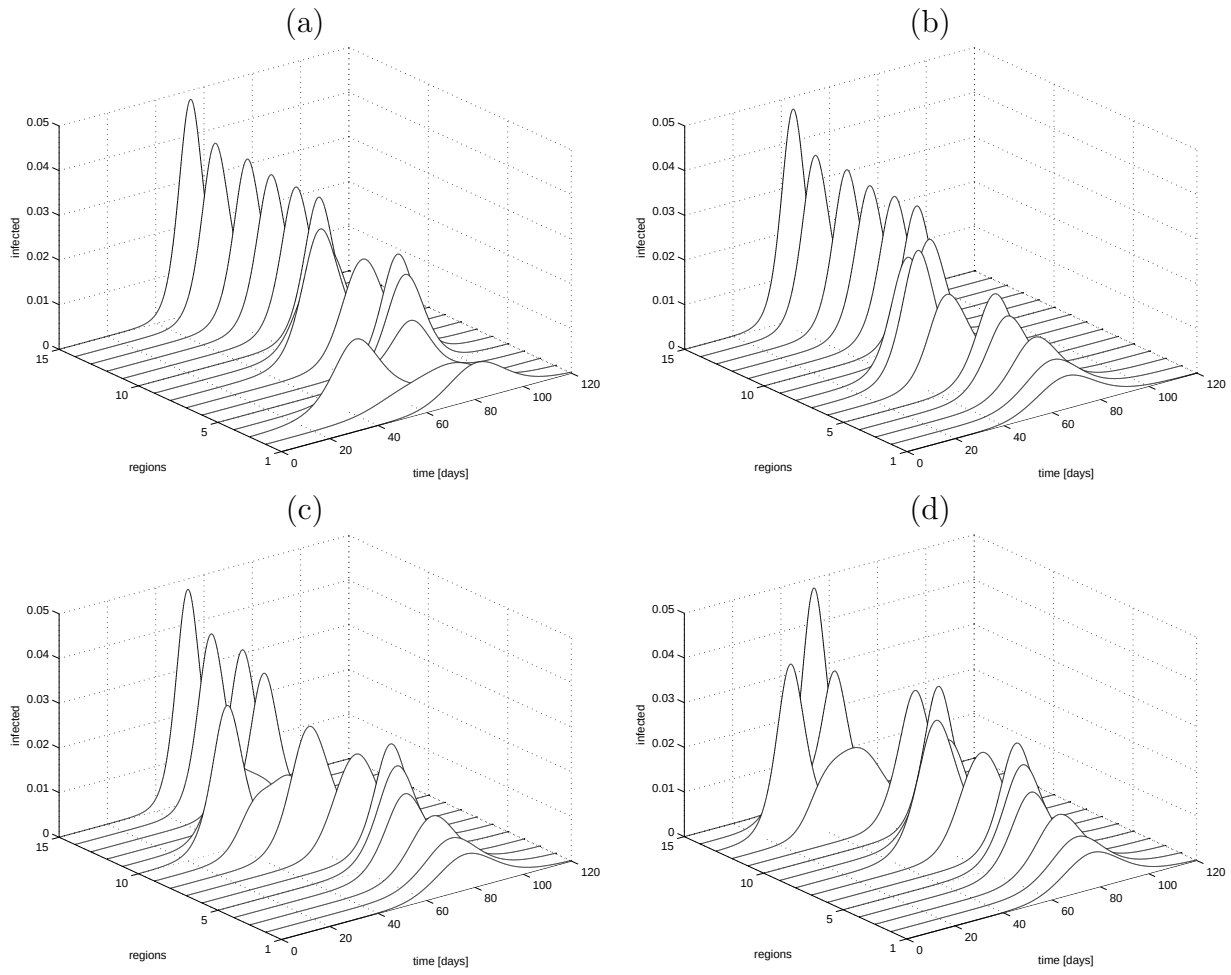

FIGURE 3. Simulation of disease spread for four different initial scenarios; same results as in Figure 2 but normalized by the number of inhabitants in each region: (a) Scenario 3, (b) Scenario 7, (c) Scenario 10, (d) Scenario 13.

Finally, we display in Figure 5 the computed peak timing for the model (2.2) (without a hub region) and the diffusion coefficient $d = 1000\,\mathrm{km^2 d^{-1}}$, which is much larger than the one used before and has been chosen so that the time frame of the peak timing of the epidemic resembles that of the experimental data.

4.4. **Case $R_0(x) < 1$ for $x \in [0, L/2)$ and $R_0(x) \geq 1$ for $x \in [L/2, L]$.** In this case, the local transmission coefficient $\beta(x)$ is set so that $R_0(0) = 0.8$ (northernmost region) and that increases linearly as a function of space until $R_0(L) = 1.2$ (southernmost region), i.e.,

$$\beta(x) = \frac{x}{10L} + 0.2, \quad 0 \leq x \leq L.$$

The parameters for diffusion and local-migration are $d = 1000\,\mathrm{km^2 d^{-1}}$ and $\nu = 2 \times 10^{-4}\,\mathrm{d^{-1}}$.

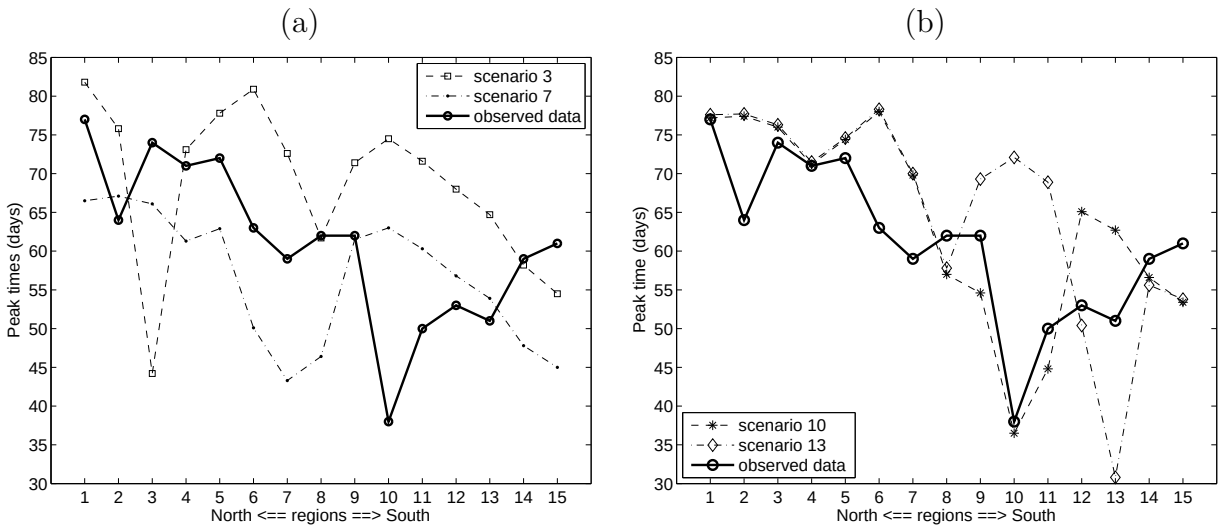

FIGURE 4. Simulated region-wise peak timing for different scenarios with $d = 10\,\mathrm{km^2 d^{-1}}$, $R_0(x) > 1$ for $x \in [0, L]$, and including a hub region (region 7) with $\nu = 10^{-5}\mathrm{d}^{-1}$.

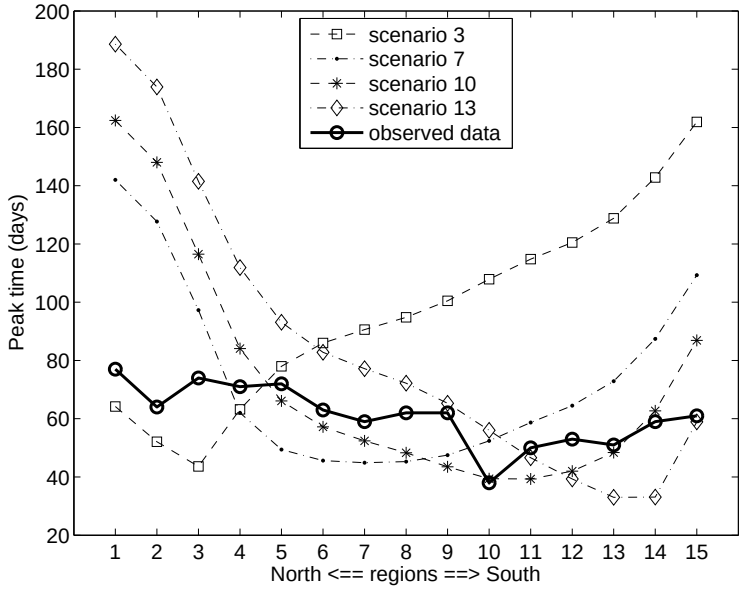

FIGURE 5. Simulated region-wise peak timing for different scenarios with $d = 1000\,\mathrm{km^2 d^{-1}}$, $R_0(x) > 1$ for $x \in [0, L]$, without a hub region.

In Figure 6 the newly infected individuals at each regions are shown. It is remarkable that an epidemic in the northern regions is triggered from an epidemic from the southern regions, even when the corresponding R_0 is less than one.

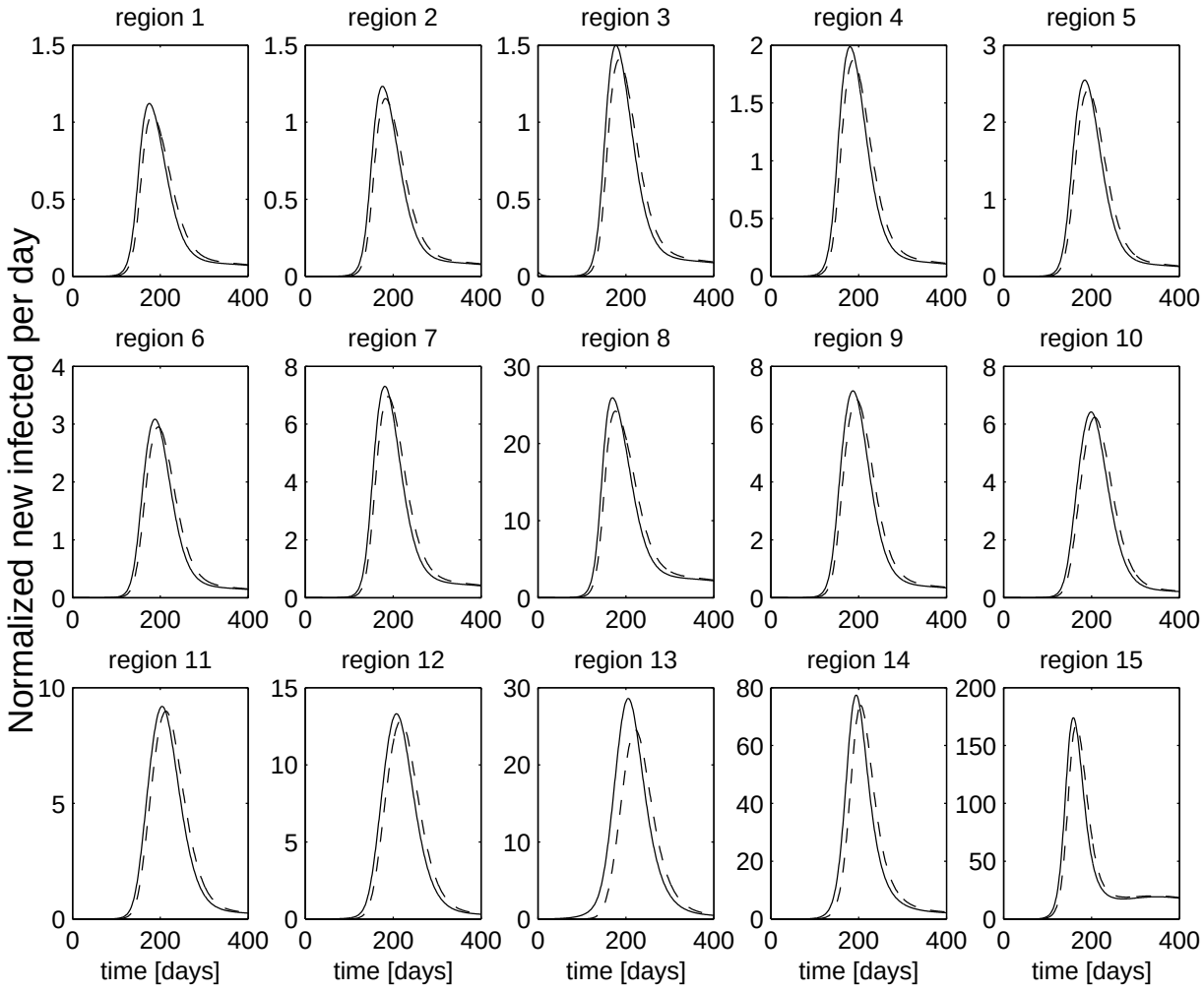

FIGURE 6. Simulation new infected $I_i^{\text{new}}(t)$ for each region i for scenario 3 (dashed curves) and scenario 13 (solid curves) for $d = 1000\,\text{km}^2\text{d}^{-1}$, a hub region with $\nu = 2 \times 10^{-4}\,\text{d}^{-1}$, $R_0(x) < 1$ for $x \in [0, L/2)$ and $R_0(x) \geq 1$ for $x \in [L/2, L]$.

5. Conclusions and discussion

We have used epidemic modeling to gain a better understanding of the spatial-temporal pattern associated with the 2009 A/H1N1 influenza pandemic in Chile. Our results show that a relatively simple spatial SEIR transmission model with a single hub representing the highly connected metropolitan region is able to reproduce the qualitative characteristics of the spreading pandemic wave in Chile (see Figures 2 and 3). These results further support that the SEIR model is a suitable basis for the description of the 2009 influenza A/H1N1; see [32] for a compartmental version of this model applied to describe the spread of this disease in Japan. Moreover, our findings suggest that the south-north gradient in pandemic peaking timing observed in Chile in 2009 is robust to variations in the initial conditions (e.g., location

of initial infectious cases) as long as the local basic reproduction number follows an increasing trend from south to north based on earlier estimations in [14]. Importantly, our results suggest that future influenza pandemics could follow similar spatial temporal dynamics to that of the 2009 A/H1N1 influenza pandemic. Our findings could have implications for pandemic preparedness and control of future influenza pandemics.

Our results indicate that the hub region that corresponds to the metropolitan region of Chile plays the critical role in keeping the entire population well mixed in a relatively short period of time. Hence, the infection is quickly spread across the entire territory as soon as the initial cases are seeded in any region of the country (Figure 4). Overall, the peak timing tended to occur first in the region where the initial cases were first introduced, but it then rapidly spread throughout the country and was locally modulated by the corresponding transmissibility level as measured by R_0 in each region, and followed a decreasing trend of R_0 from the southernmost to the northernmost regions of Chile. Our results also showed that even when the region-specific R_0 is set to values less than one, it is possible to generate small outbreaks via frequent importation of exposed individuals, through the hub, from other regions that support epidemic outbreaks, see Figure 6. In contrast to the transmission mode with hub, our transmission model with spatial local diffusion alone was not able to generate pandemic profiles that were qualitatively consistent with the 2009 A/H1N1 pandemic data from Chile obtained in [14]. Specifically, the results obtained using the diffusion model were quite sensitive to the initial region where the first cases were introduced as shown in Fig 5. Perhaps not surprisingly the spatial model with diffusion generated the best fits to peak timing data when the initial cases were introduced in the southernmost regions of Chile. However, even in these scenarios the spreading pandemic wave took a considerable amount of time to reach the northernmost regions (over 140 days compared with about 78 days from actual pandemic data).

It is interesting that the south-north spreading wave of 2009 pandemic activity in Chile is reminiscent of the spread of the 2009 pandemic in Brazil, with the southernmost regions of this country being hit earlier and experiencing greater severity than northern regions [33]. We hypothesize that our transmission model with a hub represented by the highly connected areas of the south of Brazil (e.g., São Paulo, Rio do Janeiro) and a similar south-north gradient in transmissibility could be able to generate a qualitatively similar pattern to that observed in 2009 in that country. By contrast, seasonal influenza has been observed to originate from low-population regions in the equatorial north of Brazil and travel to highly populous regions in the subtropical south over a 3-month period [34], together with a weak transmissibility gradient [35].

Although we have focused on characterizing the pandemic peak timing of the spreading wave, the timing of pandemic onset could not be well characterized using out dataset of severe acute respiratory infections (SARI), which tend to capture the highest levels of the severity pyramid. As previously reported [14], the metropolitan region experienced early introductions of the A/H1N1 influenza virus in May 2009, but local outbreaks did not immediately followed, which suggest that local climatic conditions at the time did not enable widespread transmission in the region. Instead, epidemiological investigations revealed that the well-connected southern city of Puerto Montt experienced full-scale transmission of novel

A/H1N1 influenza as of late April 2009 before the confirmation of the first case in the country [16]. This suggests that local climatic conditions played a significant role in facilitating the onset of the 2009 A/H1N1 influenza pandemic by modulating the timing of a shift of the basic reproduction number from $R_0 < 1$ to $R_0 > 1$.

It is worth noting that we did not attempt to quantify the exact magnitude and progression of the spread of the 2009 A/H1N1 influenza pandemic because our SARI data only allowed the approximate identification of the timing of evolution of the pandemic (e.g. peak timing) rather than an accurate assessment of the onset, peak timing, and duration. Furthermore, the quantification of the magnitude of the pandemic in terms of attack rates would require more complex models than those employed here. For instance, we did not model the effect of winter vacation periods although it has been reported that the school break took place after the pandemic had reached peak levels in most parts of the country [14]. In addition, we did not account for the high rates of antiviral use in Chile, a country where treatment with oseltamivir was recommended for all symptomatic individuals older than 5 years that complied with the influenza clinical case definition [16].

Our findings could have important implications for pandemic preparedness as our results suggest that future influenza pandemics could follow similar spatial temporal dynamics to that of the 2009 A/H1N1 influenza pandemic. Intensified surveillance strategies in southern regions could lead to earlier detection of novel influenza viruses.

Acknowledgements

RB acknowledges support by Fondecyt project 1130154; Conicyt project Anillo ACT1118 (ANANUM); Red Doctoral REDOC.CTA, MINEDUC project UCO1202 at Universidad de Concepción; BASAL project CMM, Universidad de Chile and Centro de Investigación en Ingeniería Matemática (CI^{2}MA), Universidad de Concepción; and Centro CRHIAM Proyecto Conicyt Fondap 15130015. PM is supported by Spanish MINECO project MTM2011-22741.

References

[1] J. Tamerius, M.I. Nelson, S.Z. Zhou, C. Viboud, M.A. Miller, W.J. Alonso, Global influenza seasonality: reconciling patterns across temperate and tropical regions, Environ. Health Perspect. 119 (2011) 439–445.

[2] J. Shaman, V. Pitzer, C. Viboud, B. Grenfell, M. Lipsitch, Absolute humidity and the seasonal onset of influenza in the continental United States, PLoS Biol. 8 (2010), paper e1000316.

[3] C. Jackson, E. Vynnycky, J. Hawker, B. Olowokure, P. Mangtani, School closures and influenza: systematic review of epidemiological studies, BMJ open 3 (2) (2013), paper e002149.

[4] S. Cauchemez, N. Ferguson, C. Wachtel, A. Tegnell, G. Saour, B. Duncan, A. Nicoll, Closure of schools during an influenza pandemic, Lancet Infect. Dis. 9 (2009) 473–481.

[5] C. Viboud, O.N. Bjornstad, D.L. Smith, L. Simonsen, M.A. Miller, B.T. Grenfell, Synchrony, waves, and spatial hierarchies in the spread of influenza, Science 312 (2006) 447–451.

[6] D. Balcan, H. Hu, B. Goncalves, P. Bajardi, C. Poletto, J.J. Ramasco, D. Paolotti, N. Perra, M. Tizzoni, W. Van den Broeck, V. Colizza, A. Vespignani, Seasonal transmission potential and activity peaks of the new influenza A(H1N1): a Monte Carlo likelihood analysis based on human mobility, BMC Med. 7 (2009), paper 45 (12pp).

[7] V. Colizza, A. Barrat, M. Barthelemy, A.J. Valleron, A. Vespignani, Modeling the worldwide spread of pandemic influenza: baseline case and containment interventions, PLoS Med. 4 (2007), paper e13 (16pp).

[8] J.B. Wenger, E.N. Naumova, Seasonal synchronization of influenza in the United States older adult population, PLoS One 5 (2010), paper e10187 (11pp).
[9] D.L. Schanzer, J.M. Langley, T. Dummer, S. Aziz, The geographic synchrony of seasonal influenza: a waves across Canada and the United States, PLoS One 6 (2011), paper e21471 (8pp).
[10] G. Chowell, S. Echevarría-Zuno, C. Viboud, L. Simonsen, J. Tamerius, M.A. Miller, V.H. Borja-Aburto, Characterizing the epidemiology of the 2009 influenza A/H1N1 pandemic in Mexico, PloS Med. 8 (2011), paper e1000436 (13pp).
[11] G. Chowell, C. Viboud, C.V. Munayco, J. Gomez, L. Simonsen, M.A. Miller, J. Tamerius, V. Fiestas, E.S. Halsey, V.A. Laguna-Torres, Spatial and temporal characteristics of the 2009 A/H1N1 influenza pandemic in Peru, PLoS One 6 (2011), paper e21287 (10pp).
[12] H. Yu, S. Cauchemez, C.A. Donnelly, L. Zhou, L. Feng, N. Xiang, J. Zheng, M. Ye, Y. Huai, Q. Liao, Z. Peng, Y. Feng, H. Jiang, W. Yang, Y. Wang, N.M. Ferguson, Z. Feng, Transmission dynamics, border entry screening, and school holidays during the 2009 influenza A (H1N1) pandemic, China, Emerg. Infect. Dis. 18 (2012) 758–766.
[13] L. Opatowski, C. Fraser, J. Griffin, E. de Silva, M.D. Van Kerkhove, E.J. Lyons, S. Cauchemez, N.M. Ferguson, Transmission characteristics of the 2009 H1N1 influenza pandemic: comparison of 8 Southern hemisphere countries, PLoS Pathog. 7 (2011), paper e1002225 (10pp).
[14] G. Chowell, S. Towers, C. Viboud, R. Fuentes, V. Sotomayor, L. Simonsen, M. Miller, M. Lima, C. Villarroel, M. Chiu, The influence of climatic conditions on the transmission dynamics of the 2009 A/H1N1 influenza pandemic in Chile, BMC Infect. Dis. 12 (2012), paper 298 (12pp).
[15] K. Khan, J. Arino, W. Hu, P. Raposo, J. Sears, F. Calderon, C. Heidebrecht, M. Macdonald, J. Liauw, A. Chan, M. Gardam, Spread of a novel influenza A (H1N1) virus via global airline transportation, New Engl. J. Med. 361 (2009) 212–214.
[16] E. Pedroni, M. Garcia, V. Espinola, A. Guerrero, C. Gonzalez, A. Olea, M. Calvo, B. Martorell, M. Winkler, M. Carrasco, Outbreak of 2009 pandemic influenza A(H1N1, Los Lagos, Chile, April–June 2009, Eurosurveillance 15 (2010), paper 19456 (9pp).
[17] A. Lowen, S. Mubareka, J. Steel, P. Palese, Influenza virus transmission is dependent on relative humidity and temperature, PLoS Pathog. 3 (2007) 1470–1476.
[18] A. Lowen, J. Steel, S. Mubareka, P. Palese, High temperature (30 degrees C) blocks aerosol but not contact transmission of influenza virus, J. Virol. 82 (2008) 5650–5652.
[19] S. Mubareka, A. Lowen, J. Steel, A. Coates, A. Garcia-Sastre, P. Palese, Transmission of influenza virus via aerosols and fomites in the guinea pig model, J. Infect. Dis. 199 (2009) 858–865.
[20] J. Shaman, M. Kohn, Absolute humidity modulates influenza survival, transmission, and seasonality, Proc. Natl. Acad. Sci. USA 106 (2009) 3243–3248.
[21] J. Steel, P. Palese, A. Lowen, Transmission of a 2009 pandemic influenza virus shows a sensitivity to temperature and humidity similar to that of an H3N2 seasonal strain, J. Virol. 85 (2011) 1400–1402.
[22] W.O. Kermack, A.G. McKendrick, A contribution to the mathematical theory of epidemics, Proc. Roy. Soc. A 115 (1927) 700–721.
[23] Y. Takeuchi, Y. Iwasa, K. Sato, Mathematics for Life Science and Medicine. Springer-Verlag, Berlin, 2007.
[24] R.M. Anderson, R.M. May, Infectious Diseases of Humans: Dynamics and Control, Oxford Science Publications, 1991.
[25] E. Vynnycky, R.E. White, An Introduction to Infectious Disease Modelling, Oxford University Press, 2010.
[26] F. Brauer, C. Castillo-Chavez, Mathematical Models in Population Biology and Epidemiology, Second Ed., Springer, New York, 2012.
[27] P. van den Driessche, Deterministic compartmental models: extensions of basic models. In F. Brauer, P. van den Driessche, J. Wu (Eds.), Mathematical Epidemiology, Springer-Verlag, Berlin, 2008, 147–157.
[28] O. Diekmann, H. Heesterbeek, T. Britton, Mathematical Tools for Understanding Infectious Disease Dynamics, Princeton Series in Theoretical and Computational Biology, Princeton University Press, 2012.

[29] L. Sattenspiel, The Geographic Spread of Infectious Diseases: Models and Applications, Princeton Series in Theoretical and Computational Biology, Princeton University Press, 2009.
[30] R. Bürger, P. Mulet, L.M. Villada, Regularized nonlinear solvers for IMEX methods applied to diffusively corrected multi-species kinematic flow models, SIAM J. Sci. Comput. 35 (2013) B751–B777.
[31] Instituto Nacional de Estadísticas (INE). Estadísticas Demográficas y Vitales, 2009. Available from: http://www.ine.cl/canales/chile_estadistico/demografia_y_vitales/demo_y_vita.php
[32] M.M. Saito, S. Imoto, R. Yamaguchi, H. Sato, H. Nakada, M. Kami, S. Miyano, T. Higuchi, Extension and verification of the SEIR model on the 2009 influenza A (H1N1) pandemic in Japan, Math. Biosci. 246 (2013) 47–54.
[33] C. Schuck-Paim, C. Viboud, L. Simonsen, M.A. Miller, F.E. Moura, R.M. Fernandes, M.L. Carvalho, W.J. Alonso, Were equatorial regions less affected by the 2009 influenza pandemic? The Brazilian experience. PLoS One 7 (2012), paper e41918 (10pp).
[34] W.J. Alonso, C. Viboud, L. Simonsen, E.W. Hirano, L.Z. Daufenbach, M.A. Miller, Seasonality of influenza in Brazil: a traveling wave from the Amazon to the subtropics, Amer. J. Epidemiol. 165 (2007), 1434–1442.
[35] G. Chowell, C. Viboud, L. Simonsen, M. Miller, W.J. Alonso, The reproduction number of seasonal influenza epidemics in Brazil, 1996–2006, Proc. Biol. Sci. 277 (2010) 1857–1866.

Centro de Investigación en Ingeniería Matemática (CI^{2}MA)

PRE-PUBLICACIONES 2013 - 2014

2013-18 Fernando Betancourt, Raimund Bürger, Stefan Diehl, Sebastian Farås: *A model of clarifier-thickener control with time-dependent feed properties*

2013-19 Gabriel N. Gatica, Antonio Marquez, Ricardo Oyarzúa, Ramiro Rebolledo: *Analysis of an augmented fully-mixed approach for the coupling of quasi-Newtonian fluids and porous media*

2013-20 Sergio Caucao, David Mora, Ricardo Oyarzúa: *Analysis of a mixed-FEM for the pseudostress-velocity formulation of the Stokes problem with varying density*

2013-21 Erwan Hingant, Mauricio Sepúlveda: *On a sorption-coagulation equation: statement, existence and numerical approximation*

2013-22 Veronica Anaya, Mostafa Bendahmane, Michael Langlais, Mauricio Sepúlveda: *A convergent finite volume method for a model of indirectly transmitted diseases with nonlocal cross-diffusion*

2013-23 Tomás Barrios, Rommel Bustinza, Víctor Domínguez: *On the discontinuous Galerkin method for solving boundary problems for the Helmholtz equation: A priori and a posteriori error analyses*

2013-24 Aníbal Coronel, Patricio Cumsille, Mauricio Sepúlveda: *Convergence of a level-set algorithm in scalar conservation laws*

2013-25 Salim Meddahi, David Mora, Rodolfo Rodríguez: *Finite element analysis for a pressure-stress formulation of a fluid-structure interaction spectral problem*

2013-26 Fabián Flores-Bazán, Fernando Flores-Bazán, Sigifredo Laengle: *Characterizing efficiency on infinite-dimensional commodity spaces with ordering cones having possibly empty interior*

2014-01 Alfredo Bermúdez, Dolores Gómez, Rodolfo Rodríguez, Pablo Venegas: *Mathematical analysis and numerical solution of axisymmetric eddy-current problems with Preisach hysteresis model*

2014-02 Carolina Dominguez, Gabriel N. Gatica, Salim Meddahi: *A posteriori error analysis of a fully-mixed finite element method for a two-dimensional fluid-solid interaction problem*

2014-03 Raimund Bürger, Gerardo Chowell, Pep Mulet, Luis M. Villada: *Modelling the spatial-temporal evolution of the 2009 A/H1N1 influenza pandemic in Chile*

Para obtener copias de las Pre-Publicaciones, escribir o llamar a: Director, Centro de Investigación en Ingeniería Matemática, Universidad de Concepción, Casilla 160-C, Concepción, Chile, Tel.: 41-2661324, o bien, visitar la página web del centro: `http://www.ci2ma.udec.cl`







Centro de Investigación en
Ingeniería Matemática (CI²MA)
Universidad de Concepción

Casilla 160-C, Concepción, Chile
Tel.: 56-41-2661324/2661554/2661316
http://www.ci2ma.udec.cl